

DTC strategy for a DSP-based Five-Level Flying-Capacitor Drive with improved flux estimation

Abstract. This paper gives a detailed analysis of direct torque control (DTC) strategy in a five-level drive and proposes a 24-sector switching table. Also, flux estimation has been improved by a discrete-time low-pass filter (LPF) with variable cut-off frequency. Algorithm to compensate the amplitude and phase errors is introduced and algorithm to determine digital filter coefficients at different speeds is presented. Simulation and practical results on a prototype using an induction motor 400V, 3kVA are given. To implement the DTC strategy, processor TMS320F2812 is used.

Streszczenie. Przedstawiono analizę strategii DTC w napędzie pięciopoziomowym i zaproponowano 24-sektorową tabelę przełączzeń. Strumień był ulepszony dzięki zastosowaniu cyfrowego filtra dolnoprzepustowego o różnej częstotliwości odcięcia. Wprowadzono algorytm kompensacji błędu amplitudy i fazy dla różnych prędkości. Przeprowadzono symulację i badania prototypu dla silnika indukcyjnego 400 V, 3 kVA. Wykorzystano procesor TMS320F2812. (Strategia DTC w pięciopoziomowym napędzie wspomagany przez procesor sygnałowy)

Keywords: direct torque control, switching table, flying capacitor multilevel inverter, flux estimation.

Słowa kluczowe: bezpośrednią kontrolą momentu DTC, napęd.

Introduction

Nowadays, high power medium voltage drives are widely used in petrochemical, transportation, cement and steel industries. Research in the field of improving performance and increasing power of these medium voltage drives is increased and in the last decade it has been one of the most active areas of power electronics. Development of these drives began in last decade using the GTO and today IGCT and high voltage IGBT with the improved switching features, simplicity of control and low losses are prominent choices [1]. Although numerous structures are provided for medium voltage drives, three structures of diode-clamped, H-bridge and flying capacitor find more application and are commercially available [2]-[5]. Among the above structures, the flying capacitor inverter as shown in Fig. 1 has been noteworthy because it does not require a transformer as H-bridge inverter and it does not cause distortion as diode-clamped. It is more attractive at high switching frequencies where leads to low capacitor values. Among the methods of induction motor speed control, direct torque control (DTC) strategy with a high performance level in the low-voltage drives, also has been implemented in multilevel drives [6]-[9].

One crucial point is that DTC drive performance depends on the speed and accuracy of flux estimation. The stator flux is generally estimated using the voltage model [10]-[13]. In this model, the stator flux is achieved by the integration of back-EMF and only the measurable electrical parameters (voltage and current) in addition to the stator resistance are required. On the other hand, measuring voltage and current is always associated with dc offset. A small dc offset, no matter how small it is, can drive the pure integrator into saturation and degrade the drive performance, especially at low speeds. To solve this problem there are two common methods: using the current model and using the LPF instead of pure integrator in the voltage model. The current model avoids the drawbacks of pure integration. However, it requires accurate values for the rotor parameters and the motor speed. Rotor parameters are not directly measurable and depend on the operating conditions (temperature and magnetic saturation level). Also, the speed measurement needs an encoder which will reduce the drive reliability. On the other hand, the voltage model offers distinct advantages compared with the current model. The main advantage of the voltage model is that it does not need the rotor parameters. Also, only one parameter (the stator resistance) needs to be known. The stator resistance can be

measured quite accurately and its variations can be estimated in real time using stator-mounted temperature sensors. So in this paper, an LPF-based voltage model is used. The paper contribution is as follow. First, it gives a detailed analysis of DTC for a five level drive and how to design the related switching tables. Then, a discrete-time LPF with variable cut-off frequency suitable for flux estimation is introduced and a routine to determine the filter coefficients is given.

Direct Torque Control for Multilevel Drives

This section is devoted to the analysis of DTC for a five level drive.

A. Principles

In a three-phase symmetrical induction motor, electromagnetic torque can be expressed by:

$$(1) \quad T_e = \frac{3}{2} p \frac{L_m}{\sigma L_s L_r} |\bar{\psi}_s| |\bar{\psi}_r| \sin \delta_\psi$$

where $|\bar{\psi}_s|$ and $|\bar{\psi}_r|$, are the stator and rotor flux amplitude respectively and δ_ψ , the angle between the two flux vectors, is called the torque angle. L_m , L_s and L_r are the magnetizing, stator and rotor inductances, respectively and σ is the total leakage factor of the motor defined as:

$$(2) \quad \sigma = 1 - \frac{L_m^2}{L_s L_r}$$

In DTC, the flux amplitude is maintained in about nominal value and the torque angle is used to control the torque according to (1). Obviously, the maximum torque is achieved for $\delta_\psi = \pi/2$.

On the other hand, the torque angle is adjustable using the stator voltage vector. Stator voltage equation is given by:

$$(3) \quad \bar{u}_s = r_s \bar{i}_s + \frac{d \bar{\psi}_s}{dt}$$

Also, (3) can be rewritten as:

$$(4) \quad \frac{d \bar{\psi}_s}{dt} = \bar{u}_s - r_s \bar{i}_s$$

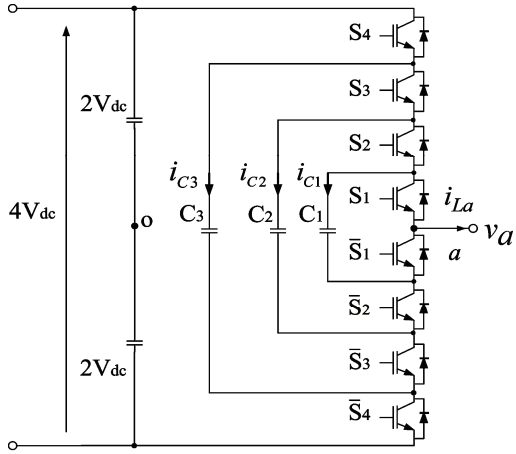


Fig.1. One leg of a five-level flying capacitor inverter

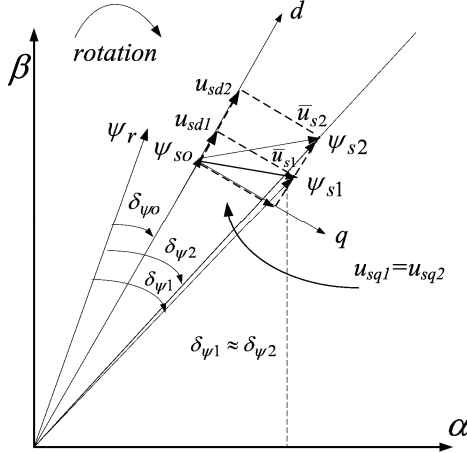


Fig.2. Impact of stator voltage vectors on torque

In multilevel drives like two-level drives, the stator flux trajectory can be controlled by selecting the appropriate stator voltage vectors. Let the rotating reference system be aligned with the stator flux vector as shown in Fig. 2, $|\bar{\psi}_s|$ (hence $|\bar{\psi}_r|$) and $\angle \bar{\psi}_s$ can be controlled by d - and q -components of \bar{u}_s , respectively. In other words, the modulus of the stator flux is affected by u_{sd} and angle of the stator flux vector is affected by u_{sq} . For instance, applying \bar{u}_{s1} and \bar{u}_{s2} vectors shown in Fig. 2, letting $u_{sq1} = u_{sq2}$, applying \bar{u}_{s1} and \bar{u}_{s2} generate the same torque. Although both vectors increase the flux amplitude, \bar{u}_{s2} leads to a faster variation in the modulus of the stator flux, since $u_{sd2} > u_{sd1}$. On the other hand, the torque angle depends on the angle of the rotor flux. The change of rotor flux position angle related to the stator current and the rotor speed is given by [14]:

$$(5) \quad \frac{d\angle \bar{\psi}_r}{dt} = \omega + \frac{L_m}{T_r |\bar{\psi}_r|} i_{sq}$$

where $\angle \bar{\psi}_r$ is the position angle of $\bar{\psi}_r$, ω is the rotor electrical speed, T_r is the rotor time constant, and i_{sq} is the q -component of \bar{i}_s with respect to the stator flux axis. \bar{u}_s develops i_{sq} with a delay related to the leakage time constant of the stator while the mechanical time constant of the drive inhibits fast change of ω . For instance, at the medium speeds a medium-size u_{sq} can increase the torque angle and consequently the amount of torque, while at high speeds the same u_{sq} causes the torque to be reduced. Therefore the vector selection will be related to the rotor

speed.

Since there are four hexagons in $\alpha\beta$ -plane, the zero speed to nominal speed can be divided into four ranges as (6): very low, low, medium and high speeds (ω_m is the rotor angular speed and ω_{nom} is nominal rotor angular speed):

$$(6) \quad \begin{cases} 0 \leq \omega_m < \omega_{nom}/4 \\ \omega_{nom}/4 \leq \omega_m < \omega_{nom}/2 \\ \omega_{nom}/2 \leq \omega_m < 3\omega_{nom}/4 \\ 3\omega_{nom}/4 \leq \omega_m \leq \omega_{nom} \end{cases}$$

B. Switching table design

The stator voltage vector in a multilevel drive is given by the well-known relation:

$$(7) \quad \bar{u}_s = u_a e^{j0} + u_b e^{j2\pi/3} + u_c e^{j4\pi/3}$$

This space voltage vector can be indicated as number cba in which a , b and c , respectively, show the voltage levels in the related phase. All the space voltage vectors for a five-level drive except the redundant vectors are shown in Fig. 3. Compared to two-level inverters, multilevel inverters have a high number of voltage vectors with different sizes so that the flux vector can be accurately controlled. Thus multilevel drives have a faster and more precise control on the flux and torque.

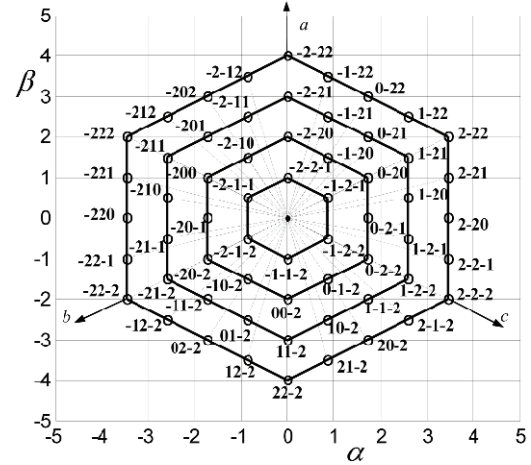


Fig.3. Voltage space vectors in a five-level inverter

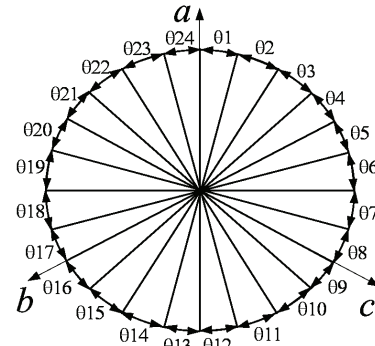


Fig.4. 24-sectors division for a multilevel inverter

As shown in Fig. 3, voltage vectors are inscribed in four hexagons. Since in the outer hexagon there are 24 voltage vectors, in this paper $\alpha\beta$ -plane is divided into 24 sectors as shown in Fig.4. Flexibility and only one-level transition during sector variation are the important advantages of a 24-sector switching table. In order to design the switching

table, the impact of different voltage vectors on torque is investigated. Here, switching table design in high speeds is presented. For instance, assume that the stator flux vector is located in sector 01 along the a -axis. In this case, all vectors in $\alpha > 0, \beta \geq 0$ increase the flux amplitude and all vectors in the region $\alpha > 0, \beta < 0$ cause the flux amplitude to decrease. Among these vectors, the group vectors 0-2x, 1-2x and 2-2x, respectively, result in a small, medium and large variation in the stator flux angle $\angle \bar{\psi}_s$. Therefore, these groups can decrease, keep constant or increase the electromagnetic torque, respectively. Among a group of vectors, a vector with a low d -component is preferred because a large d -component causes the rapid flux variation and increases the torque ripple. Although the torque ripple can be decreased by increasing the switching frequency, it is not desirable due to the loss. Vectors with a low d -component are shown in Fig. 5. Therefore, the proposed switching sequence will be as Table 1 in which the small-, medium- and large vectors are selected to reduce, keep constant or increase torque, respectively. TI and FI indexes are related to the torque and flux errors. A value of '1' or '-1', respectively, means that the desired quantity exceeds and '0' means that it is within the range. Similarly, the tables for other speeds can be provided.

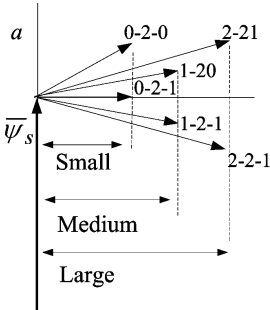


Fig.5. Selected vectors based on low d -component in sector 01

Flux estimation using the voltage model

Block diagram of direct torque control strategy is shown in Fig. 6. As mentioned before, DTC performance depends on the speed and accuracy of the torque and flux estimator.

Table 1. 24-sector switching Table in high speeds

TI	FI	01	02	03	04	05	06	07	08	09	010	011	012	013	014	015	016	017	018	19	20	21	22	23	24				
1	1	0-2-2	0-2-2	0-1-2	0-1-2	00-2	00-2	-10-2	-10-2	-20-2	-20-2	-20-1	-20-1	-200	-200	-2-10	-2-10	-2-20	-2-20	-1-20	0-20	0-20	0-2-1	0-2-1	0-2-1				
1	-1	0-2-1	0-2-1	0-2-2	0-2-2	0-1-2	0-1-2	00-2	00-2	-10-2	-10-2	-20-2	-20-2	-20-2	-20-1	-20-1	-20-1	-200	-2-10	-2-10	-2-20	-2-20	-1-20	0-20	0-20	0-20			
0	1	1-2-1	1-2-1	1-2-2	1-2-2	1-1-2	1-1-2	10-2	11-2	01-2	01-2	-11-2	-11-2	-21-2	-21-2	-21-1	-21-1	-210	-211	-201	-201	-2-11	-2-21	-1-21	-1-21	0-21	1-21		
0	-1	1-2-0	1-2-1	1-2-2	1-2-2	1-1-2	1-1-2	10-2	11-2	11-2	01-2	-11-2	-11-2	-21-2	-21-2	-21-2	-21-1	-210	-211	-201	-2-11	-2-21	-2-21	-1-21	0-21	1-21	1-21		
-1	1	2-2-1	2-2-2	2-1-2	2-0-2	21-2	22-2	12-2	02-2	-12-2	-22-2	-22-1	-220	-221	-222	-222	-212	-202	-2-12	-2-22	-1-22	0-22	1-22	2-22	2-21	2-20	2-20	2-20	
-1	-1	2-2-1	2-2-2	2-2-1	2-2-2	2-1-2	2-0-2	21-2	22-2	12-2	02-2	-12-2	-22-2	-22-1	-220	-221	-222	-212	-202	-2-12	-2-22	-1-22	0-22	1-22	2-22	2-21	2-20	2-20	2-20

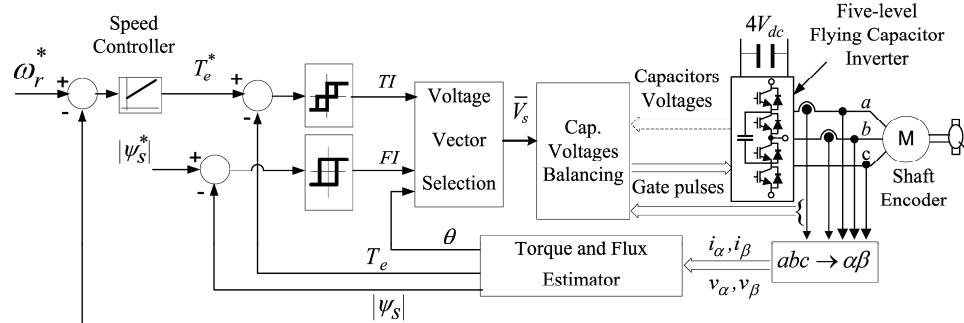


Fig.6. DTC structure in a flying capacitor inverter

The stator flux can be estimated by the voltage model or the stator voltage equation. The pure integration $1/s$ in (4) with an infinite dc gain may lead to the output saturation owing to DC offsets. To deal with the problem, the integrator is substituted with an LPF which has a limited DC gain. Frequency response of a pure integrator and the two LPFs with cut-off frequencies 2rad/sec and 20rad/sec are shown in Fig. 7. At frequencies much higher than ω_c , the LPF characteristics are similar to the pure integrator characteristics and integration runs well. However, at low frequencies there are the amplitude and phase errors. Hence, it should be noted that although with increasing ω_c the dc offset can be more attenuated, but the amplitude and phase errors will increase. The pure integrator characteristics at the stator frequency are given by $1/\omega_e$ and $-\pi/2$, respectively. The LPF transfer function and its characteristics at the stator frequency are given by:

$$(8) \quad H(s) = 1/(s + \omega_c)$$

$$(9) \quad |H(\omega_e)| = \frac{1}{\sqrt{\omega_e^2 + \omega_c^2}}$$

$$(10) \quad \angle H(\omega_e) = -\tan^{-1} \frac{\omega_e}{\omega_c}$$

Comparing two characteristics, it is clear that, the LPF leads to the amplitude and phase errors which increase with ω_c . Thus, the real stator flux amplitude is larger than the estimated value by the following factor:

$$(11) \quad \sqrt{1 + (\omega_c / \omega_e)^2}$$

So, the possibility of flux saturation is high. On the other hand due to the phase error, then $\text{Sin}\delta_{\psi_est} > \text{Sin}\delta_{\psi_real}$, that leads to the torque estimation error and increases the torque ripple. The estimated and real torques shown in Fig. 8, are given by (12).

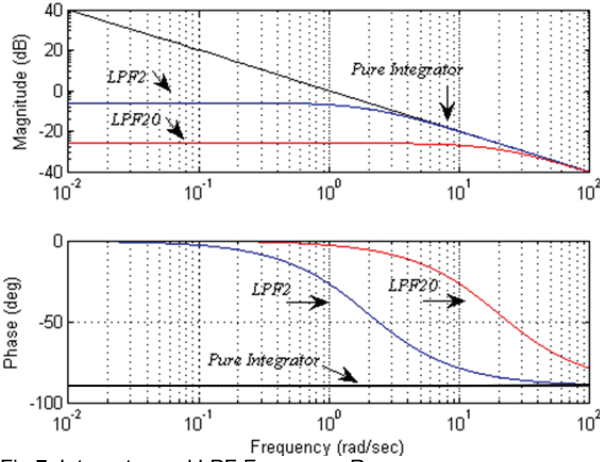


Fig.7. Integrator and LPF Frequency Response

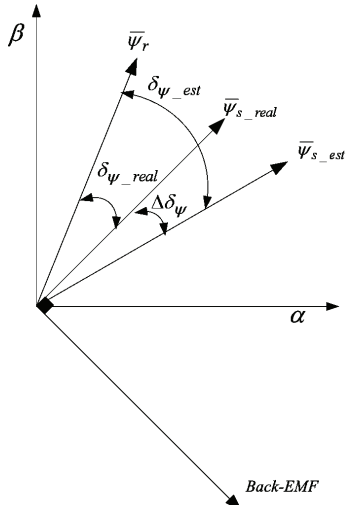


Fig.8. Flux vector and the torque angle (real and estimated)

$$(12) \quad T_{e_est} = \frac{3}{2} p \frac{L_m}{\sigma L_s L_r} |\bar{\psi}_{s2}| |\bar{\psi}_r| \sin \delta_{\psi_est}$$

$$T_{e_real} = \frac{3}{2} p \frac{L_m}{\sigma L_s L_r} |\bar{\psi}_{s1}| |\bar{\psi}_r| \sin \delta_{\psi_real}$$

Hence, the torque error is now obtained as:

$$(13) \quad \Delta T_e = T_{e_real} - T_{e_est} \propto (|\bar{\psi}_{s2}| \sin \delta_{\psi_real} - |\bar{\psi}_{s1}| \sin \delta_{\psi_est})$$

$$\Delta T_e \equiv (\sin \delta_{\psi_real} - \sin \delta_{\psi_est})$$

The torque error can degrade the drive performance especially in a high performance drive in which torque needs to be controlled. Indeed, due to the estimation error, the controller mistakenly assumes that the requested torque is generated. Torque estimation error at light loads is more important because the requested torque is about the torque error. To reduce the torque error while efficiently attenuate dc-offsets present in the back EMF, low-pass filter with a variable cut off frequency is used in which ω_c is proportional to ω_e :

$$(14) \quad \omega_c = \frac{\omega_e}{k}$$

However, amplitude and phase error still exists and an efficient integration algorithm should compensate for them. To compensate for these errors, the estimator output amplitude should be multiplied by gain (15) and its phase shifted by (16):

$$(15) \quad k_c = \sqrt{1 + (\omega_c / \omega_e)^2} = \sqrt{1 + 1/k^2}$$

$$(16) \quad \Delta \delta_{\psi} = -\frac{\pi}{2} + \tan^{-1}(k) = -\tan^{-1}(1/k)$$

Therefore, the real flux vector $\bar{\psi}_{s_real}$ can be obtained by:

$$(17) \quad \bar{\psi}_{s_real} = \bar{\psi}_{s_est} k_c (\cos \Delta \delta_{\psi} - j \sin \Delta \delta_{\psi})$$

In [10], the integration algorithm, in discrete time, is proposed as (18) with $\alpha < 1$. Also, it is suggested to reduce α with increasing the stator frequency:

$$(18) \quad y[k] = \alpha y[k-1] + x[k] \cdot T_s$$

where, x and y denote the back-EMF and the stator flux, respectively. However, the routine to calculate α and how to reduce it with increasing the stator frequency was not provided. The discrete time integration algorithm can be derived using the trapezoidal form of z :

$$(19) \quad s = \frac{2}{T_s} \frac{z-1}{z+1}$$

Substituting (19) in (8) gives:

$$(20) \quad \begin{aligned} \psi_{sd}[k] &= \alpha_1 \psi_{sd}[k-1] + \alpha_2 e_{sd}[k] \cdot T_s \\ \psi_{sq}[k] &= \alpha_1 \psi_{sq}[k-1] + \alpha_2 e_{sq}[k] \cdot T_s \end{aligned}$$

where e_{sd} and e_{sq} denote the back-EMF value in dq -coordinates and coefficients of α_1 and α_2 are given by:

$$(21) \quad \begin{cases} \alpha_1 = (1 - \omega_c T_s) \\ \alpha_2 = 1/(1 + \omega_c T_s) \end{cases}$$

The stator frequency ω_e can be obtained by:

$$(22) \quad \omega_e = \frac{(v_{qs} - i_{qs} r_s) \psi_{ds} - (v_{ds} - i_{ds} r_s) \psi_{qs}}{|\psi_s|^2}$$

Finally, the flow diagram of flux estimation is shown in Fig.9.

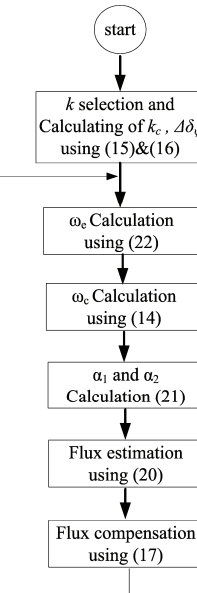


Fig.9. Flowchart for flux estimation

Simulation results

Direct torque control strategy shown in Fig. 7 is simulated and implemented using a prototype 400-volt, 3kW induction motor. Direct torque control and motor parameters are presented in the Appendix. To investigate the performance of different flux estimation algorithms, the following scenario is employed. The speed reference is set at 0.3pu and at $t = 0.15$ s, a load torque of 0.75pu is applied. Also, a 0.003pu offset is added to the measured voltage for phase a. First, the estimator with the pure integrator is simulated and the flux vector components are shown in Fig. 10. Although the estimated flux matches the real flux very well for a definite time, finally the flux saturates. Also, the torque estimation error shown in Fig. 11 is so large that the controller can't adjust the motor speed. The stator current and motor speed waveforms shown in Fig. 12 present a poor performance.

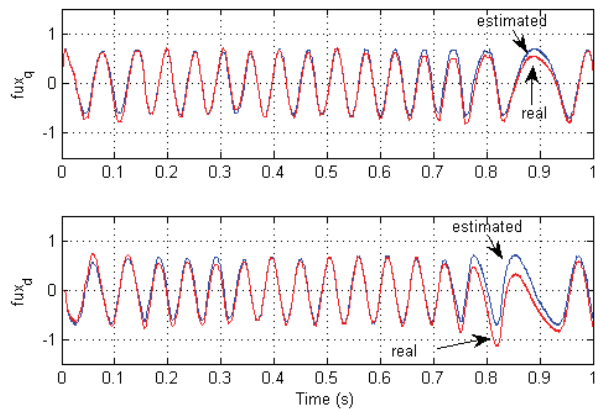


Fig.10. Real and estimated flux using a pure integrator

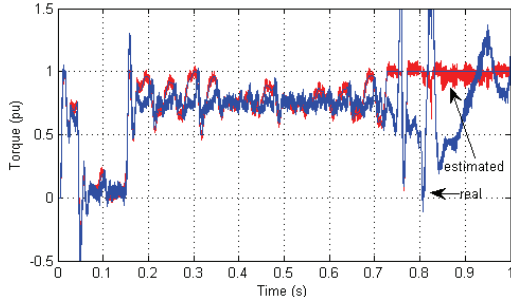


Fig.11. Real and estimated torque using a pure integrator

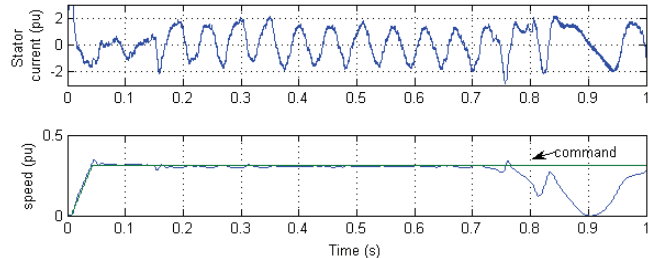


Fig.12. The waveforms using a pure integrator

Simulation results using a low-pass filter with a cut-off frequency 0.01rad/sec are shown in Fig. 13 to 15. Although the limited dc gain prevents the flux from saturation, but the phase and amplitude errors in the flux estimation, especially in the transient states, cause the torque and speed to oscillate, as shown in Fig. 14 and 15.

To avoid flux saturation, the filter cut-off frequency can be increased. Simulation results using a filter with cut-off frequency 2rad/sec is shown in Fig. 16. Although the dc offset is more attenuated but the high phase error leads to an adverse response in the transient states and the flux

saturation. Also, the flux estimation error leads to the torque estimation error as shown in Fig. 17 and system can't precisely adjust the motor speed as can be seen in Fig. 18.

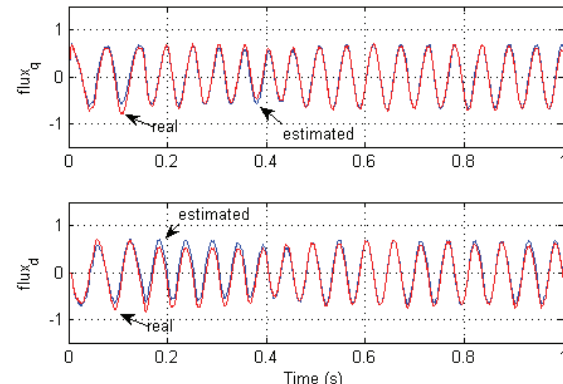


Fig.13. Real and estimated flux using LPF (0.01 rad/sec)

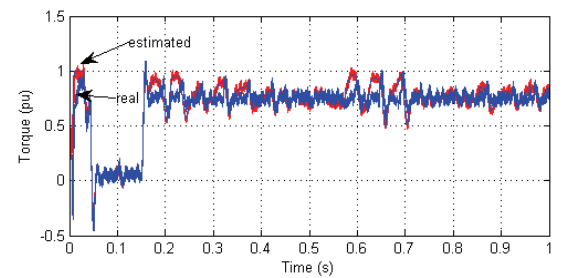


Fig.14. Real and estimated torque using LPF (0.01 rad/sec)

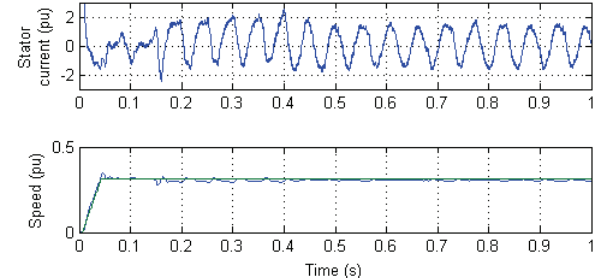


Fig.15. The waveforms using LPF (0.01 rad/sec)

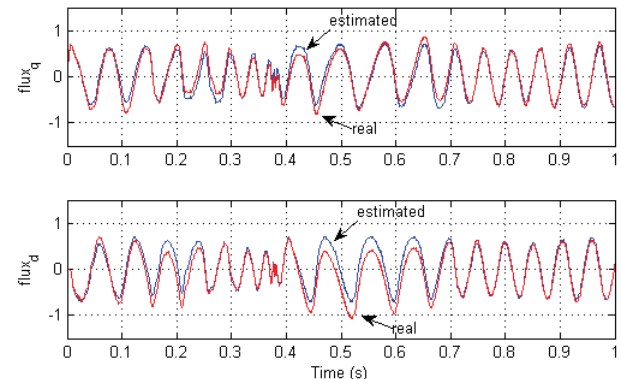


Fig.16. Real and estimated flux using an LPF (2 rad/sec)

An LPF with a variable cut off frequency is a prominent solution. The smaller k , the larger ω_c and hence the dc offset will be more attenuated. As shown in Fig. 19, for $k=2$ the estimated flux matches the real flux very well. Using the gain and the phase compensator, the estimated torque matches the real torque very well as shown in Fig. 20. The motor speed has accurately followed the speed command as can be seen in Fig. 21.

Selecting a larger k leads to reduction of the phase and amplitude error so that the transient response will be

improved. Comparing Fig. 22 with Fig. 19, the estimated flux using $k=5$ at the transient states matches the real flux very well. Also, comparing Fig. 23 with Fig. 20, it is clear that, the torque error and hence, the speed oscillations are reduced. Based on these results, k is selected between 2 and 5 depending on dc-offset values in the measured voltages.

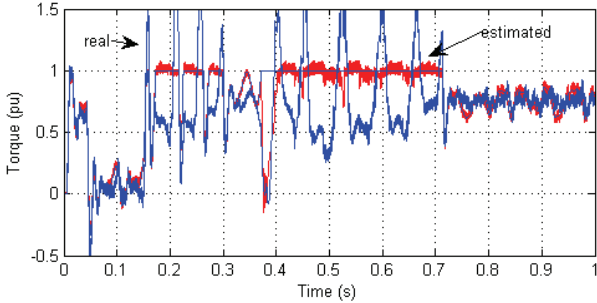


Fig.17. Real and estimated torque using LPF(2 rad/sec)

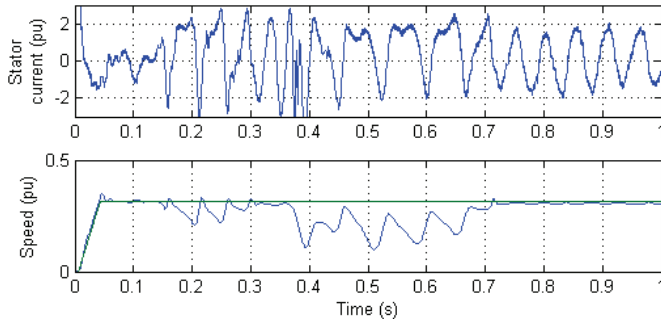


Fig.18. The waveforms using LPF (2 rad/sec)

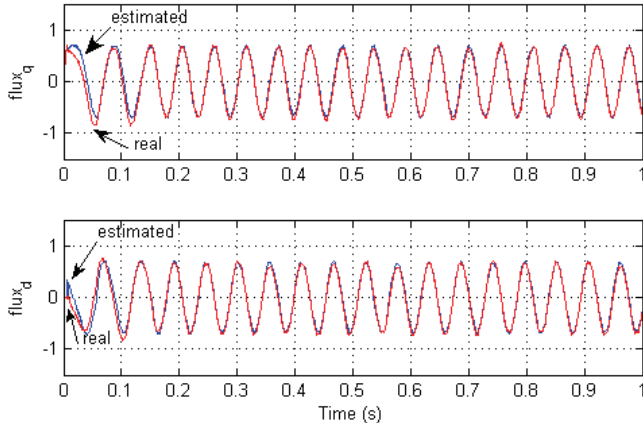


Fig.19. Real and estimated flux using variable cut-off frequency LPF with $k=2$

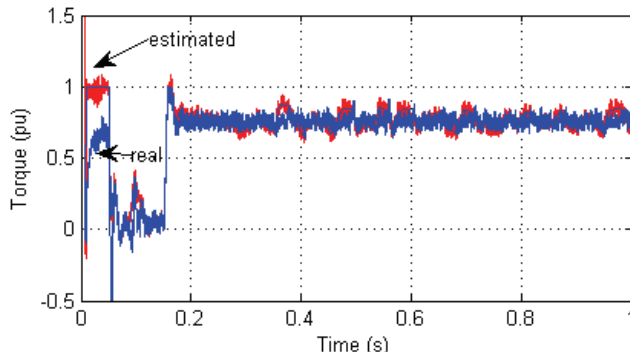


Fig. 20. Real and estimated torque using variable cut-off frequency LPF with $k=2$

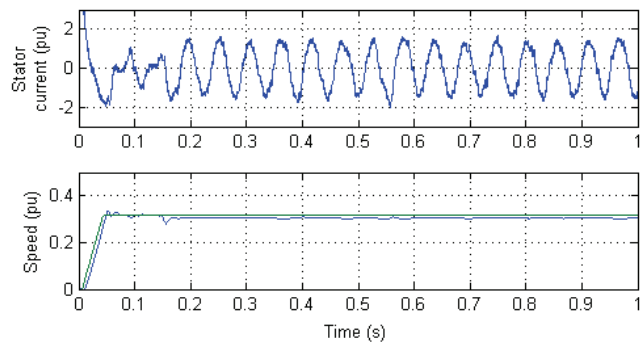


Fig.21. The waveforms using variable cut-off frequency LPF with $k=2$

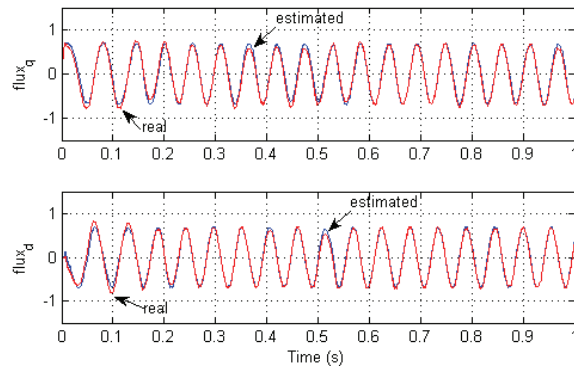


Fig.22. Real and estimated flux using a variable cut-off frequency LPF with $k=5$

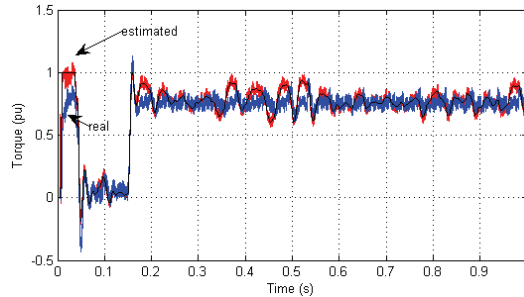


Fig.23. The waveforms torque using a variable cut-off frequency LPF with $k=5$

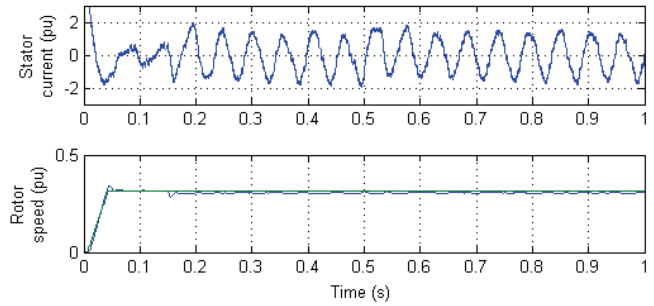


Fig.24. The stator current and rotor speed using a variable cut-off frequency LPF with $k=5$

Practical Results

Five-level flying capacitor drive is shown in Fig. 25. Different parts of the system have been named including IGBTs and related Drivers, flying capacitors, voltage transducers and DSP controller. The main processor board ezDSPF2812 with 150MIPS capability is suitable for implementing DTC. The processor is equipped with a 16-channel ADC which is used to measure nine floating-capacitor voltages, two phase-current, three-phase voltages and the DC link voltage. Six I/O port with 56-pin provides commands to 24 IGBTs easily. To measure the capacitor voltage, the isolated DC-voltage transducers are

used. A compressor shown in Fig. 26 is used as a mechanical load. The motor speed is set equal to 85% pu. First motor is started using a light-load and the estimated flux and torque are shown in Fig. 27 and 28. Reduction of the torque estimation error after compensation is evident in Fig. 28. Then, motor using the compressor as load is started and the commanded torque, the estimated torque before and after compensation, the rotor speed and the stator current as per-unit are shown in Fig. 28. In this case reduction of the torque estimation error after compensation is obvious too.

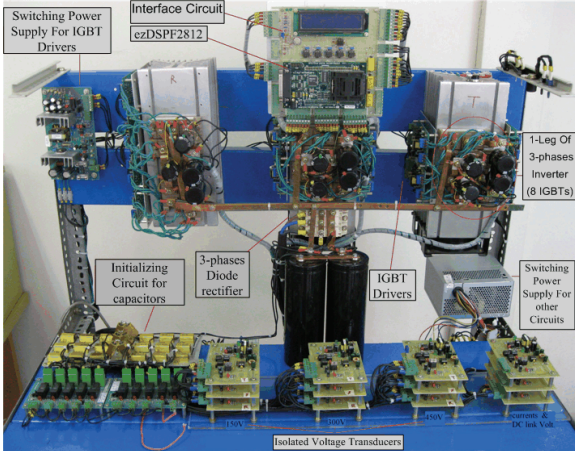


Fig.25. Five-level flying capacitor DTC drive



Fig.26. Compressor used as mechanical load

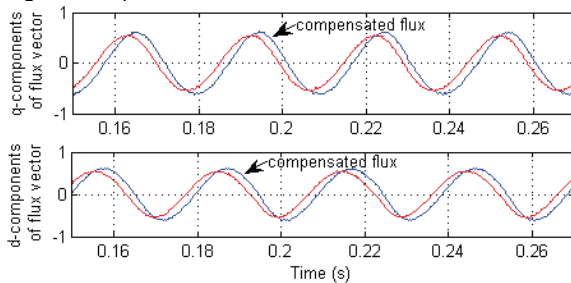


Fig.27. Estimated stator flux after and before compensation with a light load

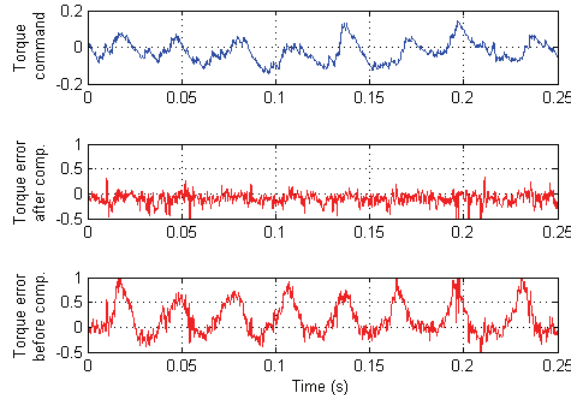


Fig.28. Torque command and its difference with estimated torque with a light load

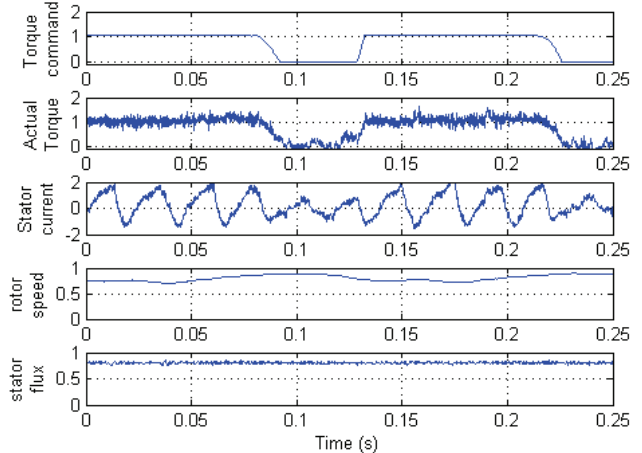


Fig.29. Torque command, actual torque, stator current, speed and stator flux with compressor load

Conclusion

This paper has analyzed in detail a 24-sector DTC strategy for a five-level flying capacitor drive and presented a proper switching table. Also, the routine to determine coefficients for the discrete time LPF is presented. The stator flux was exactly estimated by the discrete time variable-frequency LPF. Simulation and practical results on a prototype shown that using accurate flux estimation, the estimated torque matches the real torque well, especially at light loads.

Appendix

Induction motor specifications:

$V=400V$, Power=3 kW, $p=2$ (4 pole), $R_s=1.873\Omega$, $R_r=1.86\Omega$, $L_{ls}=L_{lr}=7.54mH$, $L_m=210mH$, $J=0.01kg\cdot m^2$.

Direct torque control parameters:

Torque hysteresis bandwidth = $0.2N.m$,
Flux hysteresis bandwidth = $0.01Wb$,
Initial and nominal machine flux= $0.8Wb$
Maximum switching frequency= $5000Hz$,
DTFC sampling= $50\mu s$

REFERENCES

- [1] José Rodríguez, Steffen Bernet, Bin Wu, Jorge O. Pontt and Samir Kouro, "Multilevel Voltage-Source-Converter Topologies for Industrial Medium-Voltage Drives", *IEEE Trans. Indust. Electron.*, vol. 54, no. 6, Dec. 2007
- [2] S. Kouro, M. Malinowski, K. Gopakumar, J. Pou, L. G. Franquelo, B. Wu, J. Rodriguez, M. A. Pérez, and Jose I. Leon, Member, "Recent Advances and Industrial Applications of Multilevel Converters," *IEEE Trans. Indust. Electron.*, vol. 57, no. 8, Aug. 2010
- [3] H. Abu-Rub, J. Holtz, J. Rodriguez, and G. Baoming, "Medium-Voltage Multilevel Converters—State of the Art, Challenges, and Requirements in Industrial Applications," *IEEE Trans. Indust. Electron.*, vol. 57, no. 8, Aug. 2010
- [4] S. S. Fazel, Steffen Bernet, D. Krug, and K. Jalili, "Design and Comparison of 4-kV Neutral-Point-Clamped, Flying-Capacitor, and Series-Connected H-Bridge Multilevel Converters", *IEEE Trans. Ind. Applicat.*, vol. 43, Jul./Aug. 2007 ,pp. 1032-1040.
- [5] D. Krug, S. Bernet, S. S. Fazel, K. Jalili, and M. Malinowski, "Comparison of 2.3-kV Medium-Voltage Multilevel Converters for Industrial Medium-Voltage Drives", *IEEE Trans. Indust. Electron.*, vol. 54, no. 6, Dec. 2007
- [6] J. Rodriguez, J. Pontt, S. Kouro, and P. Correa, "Direct Torque Control With Imposed Switching Frequency in an 11-Level Cascaded Inverter", *IEEE Trans. Indust. Electron.*, vol. 51, Aug. 2004 pp. 827-833.
- [7] A. Sapin, P. K. Steimer, and J.-J. Simond, "Modeling, Simulation, and Test of a Three-Level Voltage-Source Inverter

- With Output LC Filter and Direct Torque Control", *IEEE Trans. Ind. Applicat.*, vol. 43, no. 2, Mar./Apr. 2007
- [8] C. A. Martins, X. Roboam, T. A. Meynard, and A. S. Carvalho, "Switching Frequency Imposition and Ripple Reduction in DTC Drives by Using a Multilevel Converter," *IEEE Trans. Power Electron.*, vol. 17, no. 2, Mar. 2002
- [9] M.F. Escalante, J.-C. Vannier and A. Arzande, "Flying Capacitor Multilevel Inverters and DTC Motor Drive Applications", *IEEE Trans. Indust. Electron.*, vol.49, Aug. 2002, pp.809 – 815.
- [10] K. D. Husrt, T. G. Habetler, G. Griva, and F. Profumo, "Zero speed tacholess IM torque control: Simply a matter of stator voltage integration," *IEEE Trans. Ind. Applicat.*, vol. 34, pp. 790–795, Jul./Aug. 1998.
- [11] J. Hu and B. Hu, "New integration algorithms for estimating motor flux over a wide speed range," *IEEE Trans. Power Electron.*, vol. 13, pp. 969–976, Sept. 1998.
- [12] M.-H. Shin, D.-S. Hyun, S.-B. Cho, and S.-Y. Choe, "An improved stator flux estimation for speed sensorless stator flux orientation control of induction motors," *IEEE Trans. Power Electron.*, vol. 15, pp. 312–318, Mar. 2000.
- [13] N. R. N. Idris and A. H. M. Yatim, "An improved stator flux estimation in steady-state operation for direct torque control of induction machines," *IEEE Trans. Ind. Applicat.*, vol. 38, no. 1, pp. 110–116, Jan./Feb. 2002.
- [14] W. Leonhard, "Control of Electrical Drives," Third edition, Berlin, Springer, 2001.

Authors:

Mohammad Arasteh: Phd Student, marasteh@iust.ac.ir, School of Electrical Engineering, Iran University of science and technology, Narmak, Tehran, Iran.

Abdolreza Rahmati: Associate Professor, rahmati@iust.ac.ir, School of Electrical Engineering, Iran University of science and technology, Narmak, Tehran, Iran.

Shahrokh Farhangi: Professor, farhangi@ut.ac.ir, School of Electrical & Computer Engineering, University of Tehran, Tehran, Iran

Adib Abrishamifar: Assistant Professor, abrishamifar@iust.ac.ir, School of Electrical Engineering, Iran University of science and technology, Narmak, Tehran, Iran.